Physics of Fluids

RESEARCH ARTICLE | APRIL 23 2024

Analysis of the directional and spectral distributions of kinetic energy in aortic blood flow

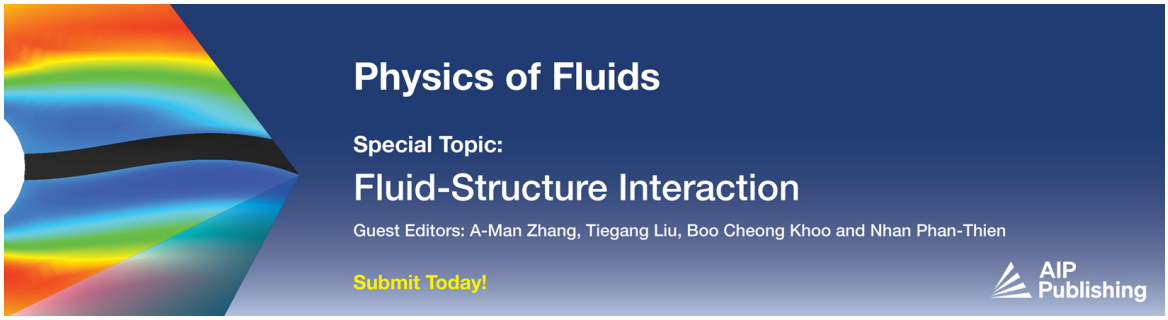
David Büchner ; Emily Louise Manchester ; Xiao Yun Xu

Check for updates

Physics of Fluids 36, 041915 (2024)
https://doi.org/10.1063/5.0203658

View Online
Export Citation

09 May 2024 15:22:56



AIP Publishing

Physics of Fluids ARTICLE pubs.aip.org/aip/pof

Analysis of the directional and spectral distributions of kinetic energy in aortic blood flow

Cite as: Phys. Fluids **36**, 041915 (2024); doi: 10.1063/5.0203658
Submitted: 15 February 2024 · Accepted: 5 April 2024 ·
Published Online: 23 April 2024

View Online Export Citation CrossMark

David Büchner,[1] Emily Louise Manchester,[1,2] and Xiao Yun Xu[1,a)]

AFFILIATIONS

[1]Department of Chemical Engineering, Imperial College London, SW7 2AZ London, United Kingdom
[2]Department of Fluids and Environment, The University of Manchester, M13 Manchester, United Kingdom

[a)]Author to whom correspondence should be addressed: yun.xu@imperial.ac.uk

ABSTRACT

It has been recognized that blood flow in large vessels, such as the aorta, may undergo a transition to turbulent flow in the presence of cardiovascular disorders, while flow in the healthy aorta is perceived to be laminar under normal physiological conditions. However, this perception has been challenged by several studies, highlighting the need to consider more fundamental flow characterizations. The present study aims to provide a comprehensive analysis of the directional and spectral distributions of kinetic energy in aortic flows under normal and pathological conditions. For this purpose, large-eddy simulation results for two patient-specific aortas, representing a healthy aorta and an aorta with aortic valve stenosis, respectively, were analyzed by decomposing the resolved transient velocity fields into directional and frequency components. It is shown that fundamental characteristics, such as the distinctive role of harmonics of the cardiac cycle as well as intermediate frequencies, indicate complex flow structures and turbulence over the entire thoracic aorta in both cases. The high-frequency components of kinetic energy are found to decrease by more than one order of magnitude from regions associated with complex flow features to the descending aorta. In conclusion, the capability of such analyses to effectively describe complex aortic blood flow at physiological and pathological conditions is demonstrated and motivates further efforts to achieve a more fundamental understanding of the true nature of aortic blood flow.

© 2024 Author(s). All article content, except where otherwise noted, is licensed under a Creative Commons Attribution (CC BY) license (https://creativecommons.org/licenses/by/4.0/). https://doi.org/10.1063/5.0203658

09 May 2024 15:22:56

I. INTRODUCTION

As the largest blood vessel in the human body, the aorta plays a central role in the cardiovascular system, and related pathologies often require complex and expensive medical interventions. With the increase in population age, the number of patients suffering from aortic diseases and aortic valve diseases is expected to rise in the coming decades.[1] Most of these diseases are associated with abnormal hemodynamics and even their progression is often linked to pathological flow patterns.[2–4]

Motivated by this, studies have been conducted to improve our understanding of hemodynamics in the aorta. In healthy aortic flow, complex flow patterns, such as systolic backflow and helical flow structure, have been identified in the ascending aorta (AAo).[5–8] In the aortic arch and the descending aorta (DAo), flow detachment and recirculation zones[9] as well as double-spiral flow[10,11] have been observed. Various aortic diseases are known to impact the flow field in the aorta, introducing additional hemodynamic complexity. For example, the skewed jet caused by aortic valve stenosis (AVS) is associated with deterioration of the aortic wall,[12] and its deflection can cause a strong helical motion in the AAo.[13–15] Such complex flow structures are often the cause of highly disturbed and turbulent flow[16] and, thus, increased shear stress, which is known to affect the functions of red blood cells[17] and endothelial cells.[18] To better quantify the associated flow parameters, patient-specific large-eddy simulation (LES) methodologies have been successfully developed to investigate transitional and turbulent flows caused by various aortic and aortic valve diseases.[16,19–21] Furthermore, it has been shown that such LES models can assist in the prediction of progressive aortic diseases and the development of concomitant disease.[22]

Despite the evidence of complex flow structures in the healthy aorta, the notion that physiological conditions are related to laminar-like flow while transition and turbulence occur in connection with pathologies remains widely accepted. This assumption persists supposedly because conventional criteria based on the Reynolds number alone cannot be applied unambiguously due to the complexity of the flow: the geometries and compliance of the vessel wall, the

© Author(s) 2024

non-Newtonian feature of the fluid, and flow pulsatility. By investigating flow in healthy carotid arteries based on Doppler ultrasound measurements and idealized Womersley flow in various blood vessels, Saqr *et al.*[23] suggest that physiological blood flow is generally turbulent. Based on their findings, the authors call for a paradigm shift and recommend that more fundamental concepts, namely chaos theory, hydrodynamic instability, and the kinetic energy cascade, should be employed to characterize turbulence in blood flow. For healthy aortas, none of the above concepts has yet been applied systematically to measurements or simulations of physiologically realistic conditions.

In classical fluid dynamics, the concept of the kinetic energy cascade describes the transfer of turbulent kinetic energy between different scales of motion and is usually characterized through the spectral distribution of the kinetic energy. Lancelotti *et al.*[24] and Mancini *et al.*[25] determined various kinetic energy spectra (KES) from simulations of flow in carotid arteries. Both studies demonstrate the need for a sufficiently fine spatial and temporal resolution of the LES to obtain a KES that reflects the expected flow characteristics. However, as their aim was to study the accuracy of different LES models, they applied constant parabolic and idealized Womersley velocity profiles at the inlets, which are known to impact the flow field significantly.[26] Only a small number of studies determined KES in blood vessels to analyze the actual nature and characteristics of the flow. This includes a range of experimental and numerical studies of the turbulence created downstream of various heart valve prostheses.[27–29] Particularly, Nitti *et al.*[27] provided a comprehensive analysis and discussion of the spectral distribution of kinetic energy and thereby successfully characterized vortex shedding and the subsequent turbulent transition behind mechanical aortic valves. However, the mentioned studies only investigated flow in the area immediately downstream of the valve and assumed either a constant flow or an idealized pulsatile inlet flow rate. In an intracranial aneurysm, Tupin *et al.*[30] applied a multi-harmonic pulsatile inlet flow rate and conducted an extensive study of the spectral distribution of kinetic energy. They found complex patterns in the KESs, such as inverse kinetic energy cascades, demonstrating the importance of this fundamental analysis to describe the flow when classical criteria are not readily applicable. A thorough literature review indicates that prior studies on the spectral distributions of kinetic energy focused on blood flow under pathological conditions. The only spectral analysis of kinetic energy in realistic healthy aortic blood flow was provided by the *in vivo* hot-film anemometer study of Stein *et al.*[31] from the 1970s. They identified differences in the KES, for example, higher amplitudes at high-frequency components in a patient suffering from AVS compared to a healthy one, but the study was limited to a small number of frequency components insufficient for a comprehensive analysis of the KES.

By conducting a systematic analysis of the directional and spectral distributions of kinetic energy over the full extent of the aorta, this study aims to improve our understanding of the complex aortic flow dynamics at physiological and pathological conditions. To this end, we used LES results obtained from two realistic models of the aorta; one representing a healthy aorta and one representing a pathological aorta. LES modeling of the aortic flow was necessary to obtain well-resolved transient velocity fields with sufficient temporal resolution for the spectral analysis. Furthermore, the LES model has been extensively validated for cardiovascular flow applications in our previous studies.[16,32] The transient velocity fields obtained from LES of both aorta models were used to determine the directional and spectral distributions of kinetic energy at various locations along the aorta. Characteristics and patterns identified in the distributions were analyzed with regard to flow structures as well as disturbances and turbulence. Insight is provided into the applicability of these methodologies to aortic flow, and a baseline case is provided for future studies on turbulence in the aorta.

II. METHODOLOGY

A. Patient-specific models and computational details

Patient-specific models of a healthy aorta and an aorta with tricuspid AVS were adopted in this study. These models, shown in Fig. 1, were built from magnetic resonance (MR) images. The corresponding 4D flow MRI data were also available and were used to provide patient-specific boundary conditions. These included time-varying, 3D velocity profiles at the ascending aorta inlet and a three-element Windkessel model at the three branch outlets and descending thoracic aorta outlet. The Windkessel model describes the ability of the circulatory system to dampen pulsatile effects, and the model is a function of pressure, flow rate, arterial compliance, and arterial resistances. The model parameters for proximal resistance, peripheral resistance, and arterial compliance are evaluated using flow data derived from a 4D flow MRI and central aortic pressure.[33] The parameters are provided in the supplementary material. The Windkessel equations are solved for pressure at each time step, resulting in a pressure waveform-type boundary condition at each outlet. The arterial wall was assumed to be rigid with a no-slip boundary condition. Full details on data acquisition, image processing, and patient-specific computational model methodologies can be found in our previous studies.[16,34] A brief summary of the computational details is given below.

Structured meshes were generated in Ansys ICEM and consisted of 7.4 and 4.5 $\times$ 10^6 cells for the AVS and healthy aorta, respectively. Detailed mesh sensitivity studies were conducted, which evaluated mesh dependence on mean and turbulence kinetic energies. For the AVS aorta, mesh sensitivity results are available in our previous publications,[16,34] and for the healthy aorta, results are included in the supplementary material. To ensure confidence in simulation accuracy, LES velocity fields were quantitatively compared with 4D flow velocity fields on a point-by-point basis using the Pearson's product-moment correlation coefficient, which gives a normalized measure of the covariance of two variables. The AVS and healthy aortas showed correlations greater than 0.7 and 0.9, respectively, for all velocity components, indicating a strong positive correlation between measured and simulated velocity fields. Full details are included in our previous study[16] and in the supplementary material.

Large-eddy simulations with the wall-adapting local eddy-viscosity (WALE) subgrid-scale model (model coefficient, $C_w = 0.325$) were performed in OpenFOAM using the pimpleFoam solver. Temporal and spatial discretization was achieved using second-order implicit backward Euler and second-order central differencing schemes, respectively. Velocity and pressure were converged to a normalized residual of 1×10^{-5} at each time step. Blood was assumed incompressible and Newtonian with density, $\rho = 1060\,\mathrm{kg/m^3}$, and dynamic viscosity, $\mu = 0.0035\,\mathrm{Pa\,s}$. A time step of 2×10^{-4} s was used, ensuring a mean CFL number less than unity throughout the cardiac cycle. Full details of the numerical approach are described in our previous publication.[16]

09 May 2024 15:22:56

© Author(s) 2024

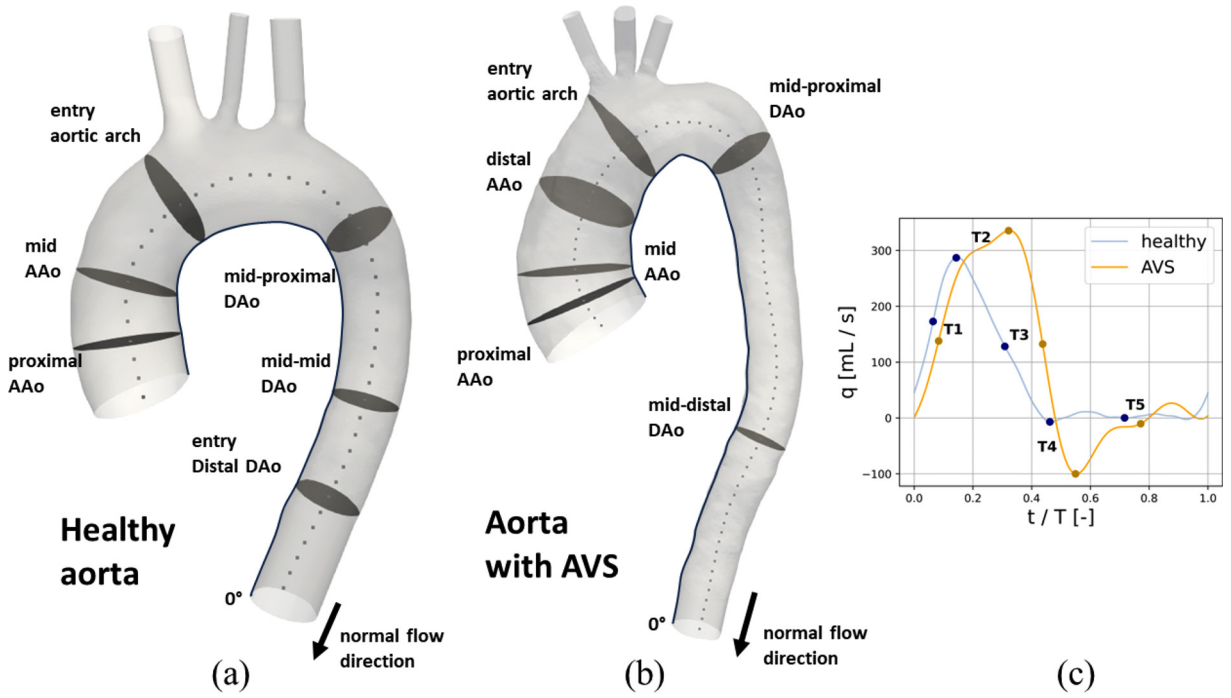


FIG. 1. Geometric models of the healthy aorta (a) and the aorta with AVS (b). The aortas are divided into ascending aorta (AAo), aortic arch, and proximal, mid, and distal descending aorta (DAo), respectively. The 0° line denotes the location of the inner curvature of the aorta. Cross sections where turbulence parameters are evaluated are indicated and the inlet flow rate waveforms for both patients are depicted (c).

B. Analysis of the flow characteristics

1. Reduction and transformation of the flow field

To facilitate spatial definition and comprehension when describing the results, the aorta is divided into sections. In consecutive order, these segments are the AAo, aortic arch, and proximal-, mid-, and distal DAo, following the naming convention introduced by Jarvis *et al.*[35] To evaluate the flow field and its spectral decomposition, six cross-sectional slices were extracted from the three-dimensional geometry of each aorta. Their locations, as shown in Fig. 1, were chosen to capture not only the most relevant flow feature, i.e., regions with vortices and separation zones, but also the dissipation of turbulence expected in their wake. The cross sections were extracted such that their normal vectors are parallel to the centerline. In turn, this allowed for a direct transformation of the velocity components from a global Cartesian system into a local cylindrical coordinate system. In these systems, the total velocity is composed of components in the normal, circumferential, and radial directions. The normal component describes the through-plane velocity, with positive values corresponding to flow downstream the aorta. The two other components describe in-plane velocities. The description of velocity in such a system is beneficial for the interpretation of the velocity field itself and for the calculation of KES.

2. Integrated kinetic energy

The integrated kinetic energy (IKE) as a quantity is not only an important measure in meteorology[36] but also finds applications in the validation of numerical flow simulation schemes.[37] Although it is not commonly used to evaluate pulsatile blood flow, its characteristics make it an ideal quantity to gain a better understanding of kinetic energy distributions in the different directions of flow in a specified volume, or in this case cross sections through the aorta. The IKE is similar to the mean kinetic energy more commonly used in cardiovascular flow research. Provided a regular Cartesian grid, with constant cell sizes, the IKE is the same as the sum of mean kinetic energy and turbulent kinetic energy. However, as the grids of the LES results adopted here are not regular, the IKE is a more accurate measure when comparing different integration volumes or surfaces. The instantaneous IKE is defined as follows:

$$IKE(t) = \frac{1}{2}\rho \int_V U(t)^2 \, dV, \tag{1}$$

where U is the velocity, ρ is the fluid density, and V is the integration volume or surface. The IKE was calculated by numerical integration of the velocity over a triangularization of the point data from LES.

3. Spectral decomposition

The spectral decomposition of the kinetic energy was performed by applying an approach previously introduced by El-Gabry *et al.*[38] to determine turbulent length scales from hot-wire velocimetry measurements. This approach was also used by Saqr *et al.*[23] to study the existence of a kinetic energy cascade primarily in the carotid artery. The local kinetic energy in the frequency domain is described as

09 May 2024 15:22:56

© Author(s) 2024

$$E_i(f) = \frac{|\Im\{u_i(t)\}|^2}{L \cdot f_s}, \tag{2}$$

where $E_i(f)$ provides the distribution of energy spectral density over the frequency f at a discrete point i. Furthermore, $\Im$ is the fast Fourier transform, u_i is the velocity signal at the given point, L is the total length of the time-discrete velocity recording, and f_s is the sampling frequency. As results obtained from LES were analyzed in this study, the sampling frequency $f_s = 100$ Hz is defined by the time interval $\Delta t = 0.01$ s at which the velocity field was saved in the output file. The length of the velocity recording, applied for normalization, is different for the healthy and diseased cases as these simulations were run for different numbers of cardiac cycles. For the healthy aorta and the aorta with AVS, the total length of time-discrete velocity recording is $L = 1945$ and $L = 2191$, respectively. It is important to note that the condition for the application of Taylor's frozen turbulence hypotheses, e.g., that turbulent fluctuations are small compared to the mean flow $\tilde{u} \ll U$, is not true for pulsatile aortic flow, and, therefore, conversion from the frequency to wavenumber domain is not possible.

III. RESULTS

A. Velocity field

To understand the spectral analysis results, first, a detailed evaluation of the flow field is carried out. Here, only the most important features are summarized, and the respective flow fields are shown in Figs. 2 and 3. Further descriptions and visualizations of the velocity fields, at all remaining cross sections, are provided in the supplementary material.

In the healthy aorta, three complex flow patterns are prominent. The first one is the formation of Dean vortices, i.e., double spiral flow, and an associated vortex structure in the AAo that develops during systolic acceleration. The vortex axis is aligned along the inner curvature of the aorta and its magnitude decreases from the AAo into the aortic arch. Although the vortex is of similar size and rotates clockwise in all cardiac cycles, its breakdown scenario during systolic deceleration varies significantly between different cardiac cycles. Weak systolic backflow is present during mid-systolic deceleration in the area previously occupied by the vortex and strongly irregular, disturbed flow, both through and in-plane, is present in the remaining area of the cross section. Further downstream, disturbed flow is also observed in the DAo. Here, the disturbance can be attributed to the continuation of the double spiral flow and the emergence of a flow detachment zone, particularly developed in the proximal DAo. Although in the mid-DAo during peak systole, an almost fully undisturbed plug flow profile develops, it appears as if the disturbances caused by the flow features in the proximal DAo during systole are not fully dissipated and transported downstream. In contrast to the AAo, however, the disturbances can dissipate almost completely in the mid-DAo during diastole. The mean and peak Reynolds numbers in the healthy aorta are 4429 and 9919, respectively, which were calculated using the mean and maximum inlet velocity at peak systole and the inlet diameter as characteristic length. The Womersley and Strouhal number are 19.2 and 0.021, respectively.

In the diseased aorta with AVS, the flow field is vastly different from the healthy aorta. This case was previously examined by Manchester *et al.*[16,34] The AVS of this patient results in a strong and inclined jet out of the aortic valve into the AAo, and the jet's impingement and deflection at the anterior aortic wall causes a strong counterclockwise rotating helical motion. Subsequently, in the AAo, most motion in the normal direction takes place along the aortic walls, while the inner areas are characterized by disturbances and partially systolic backflow. Further downstream in the DAo, regions of pronounced rotational motion are present as well; however, they are oriented in the opposite direction, e.g., clockwise. In the proximal DAo, this rotational motion appears to interfere with the formation of a detachment zone. Similarly, to the healthy aorta, the disturbances created by the various flow structures show higher dissipation levels in the DAo compared to the AAo, despite disturbances being strongest in the AAo. For the aorta with AVS, the mean and the maximum Reynolds, Womersley, and Strouhal numbers are 2375, 37 942, 43.6, and 0.017, respectively.

B. Integrated kinetic energy

The evaluation of the distribution of IKE over time and its variance over cardiac cycles allows for a better understanding of the characteristics of the flow structures found in the aorta. Figure 4 shows the IKE over the cardiac cycle and its distribution in the different spatial directions calculated for the selected cross sections along the aortas.

The plots show the phase-averaged IKE with gray bars indicating the cycle variations via one standard deviation. For the healthy aorta, it is apparent that the course of IKE in the normal (through-plane) direction is qualitatively similar to the inlet flow waveform in Fig. 1, while quantitatively the maximum IKE at the peak decreases from the proximal AAo to the distal DAo. This reflects the loss of kinetic energy due to fluid, and consequently, energy, leaving through not only the branches but also dissipation. In the circumferential direction, IKE exhibits a more complex pattern. In both the proximal- and mid-AAo, an initial peak in the circumferential direction is present right after peak systole. While in the mid-AAo, a sharp peak is observed which coincides with the time at which the vortex-like structure observed in the flow field breaks down. A slower increase following the sharp peak is characterized by overall larger cycle variations, which confirm the previous observation of considerable cycle variance differences in the breakdown scenario of the vortex and resulting disturbances. From this peak, the IKE particularly in the circumferential direction starts decreasing shortly before diastole. The somewhat more continuous and constant decrease in IKE here indicates the dissipation of kinetic energy during end-systole and diastole. Downstream, in the DAo, it can be seen that the IKE in the circumferential and radial directions is of significantly smaller magnitudes than in the AAo.

For the aorta with AVS, the IKE distribution is different than that of the healthy aorta, as can be seen in the lower row of Fig. 4. In both the normal and circumferential directions, distinctive peaks of IKE are present in the AAo. From the proximal to the distal AAo, the peak of IKE in the normal direction not only increases in magnitude but is also reached at a later relative time in the cardiac cycle. In the distal AAo, the peak is eventually reached around peak systole. In contrast, in the circumferential direction, the peak of IKE in the proximal AAo is reached at peak systole and its magnitude decreases from there while also moving to later times in the cardiac cycle. In the radial direction, the IKE peak is initially of similar magnitude as the one in the circumferential direction; however, has already declined significantly in the mid-AAo. Although the helical flow develops in all cardiac cycles similarly, it is associated with high levels of standard deviation, i.e., cycle variance, in all flow directions and particularly in the circumferential

09 May 2024 15:22:56

© Author(s) 2024

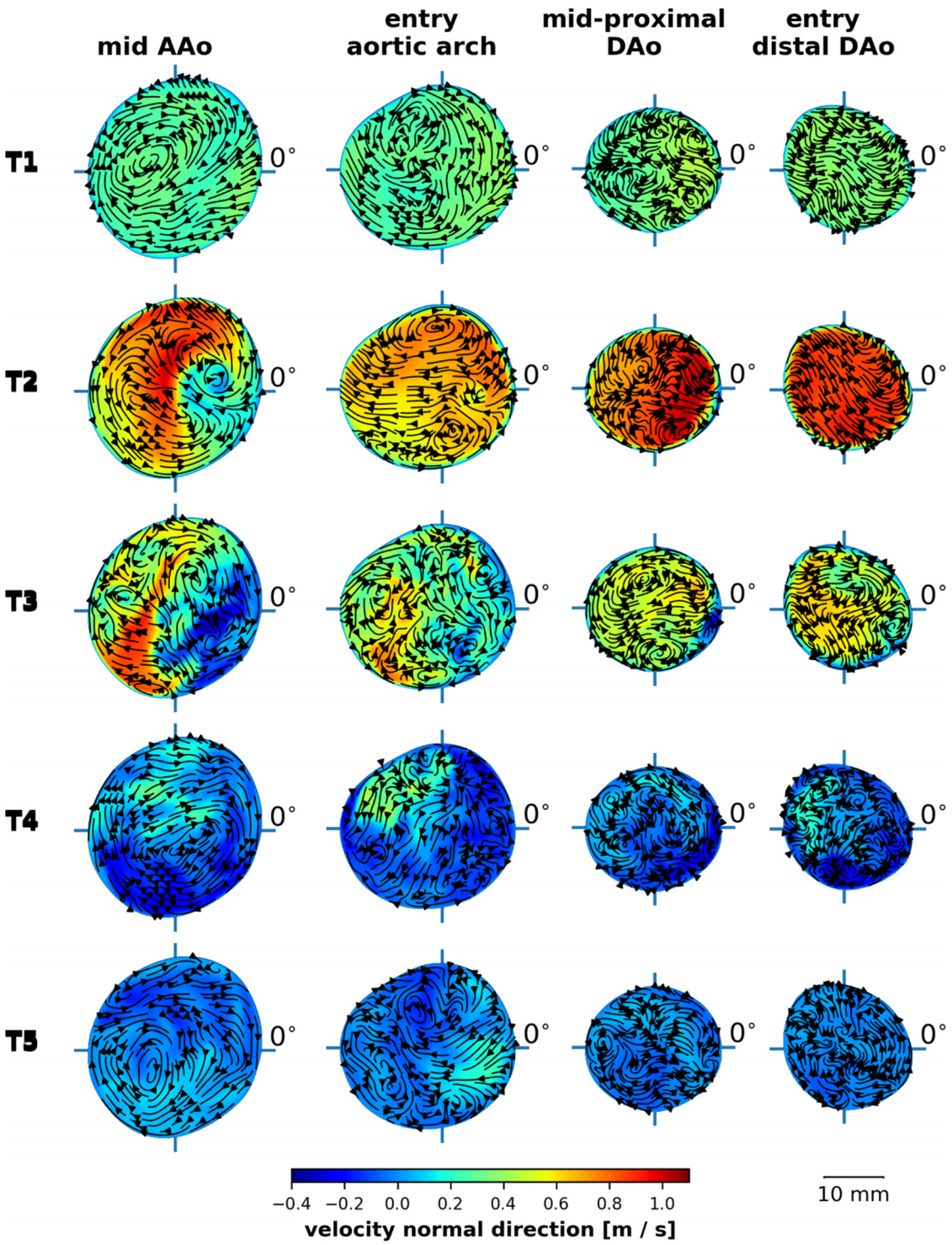


FIG. 2. Instantaneous velocity fields in the healthy aorta at different time points in one cardiac cycle. The onset of Dean vortices and highly disturbed flow can be seen in the mid-AAo and entry to the aortic arch. In the DAo, a recirculation zone is present, and the resulting disturbances remain present down to the distal DAo. The 0° markers indicate the location of the inner curvature of the aorta. T1-5 correspond to systolic acceleration, peak systole, mid-systolic deceleration, end-systole, and mid-diastole, respectively.

09 May 2024 15:22:56

© Author(s) 2024

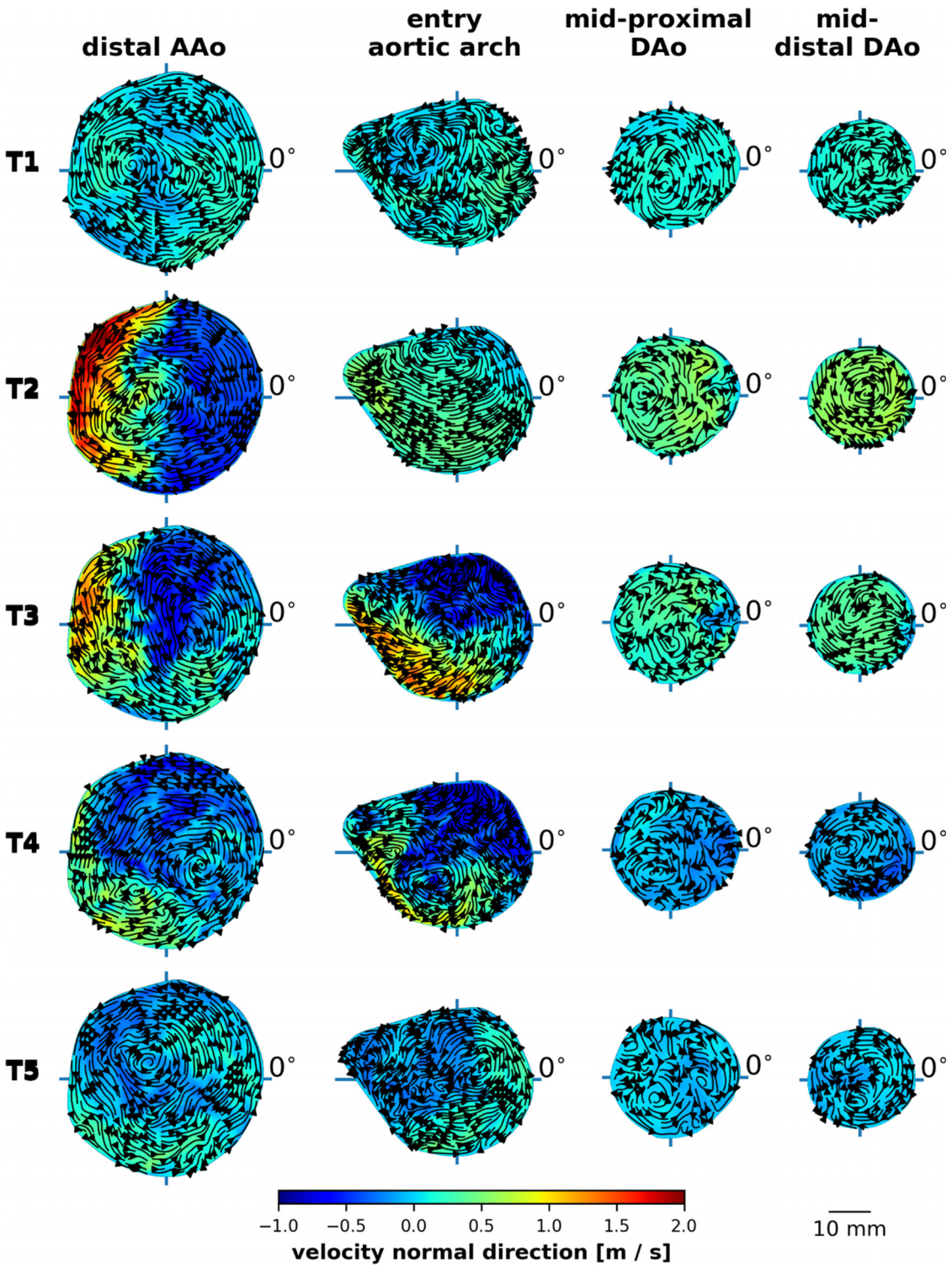


FIG. 3. Instantaneous velocity fields in the aorta with AVS at different points in the cardiac cycle. The AAo is dominated by a jet-like inflow, resulting in strong helical motion and systolic back flow. In the DAo, an additional recirculation zone is present, resulting in disturbances. The 0° markers indicate the location of the inner curvature of the aorta. T1-5 correspond to systolic acceleration, peak systole, mid-systolic deceleration, end-systole, and mid-diastole, respectively.

09 May 2024 15:22:56

© Author(s) 2024

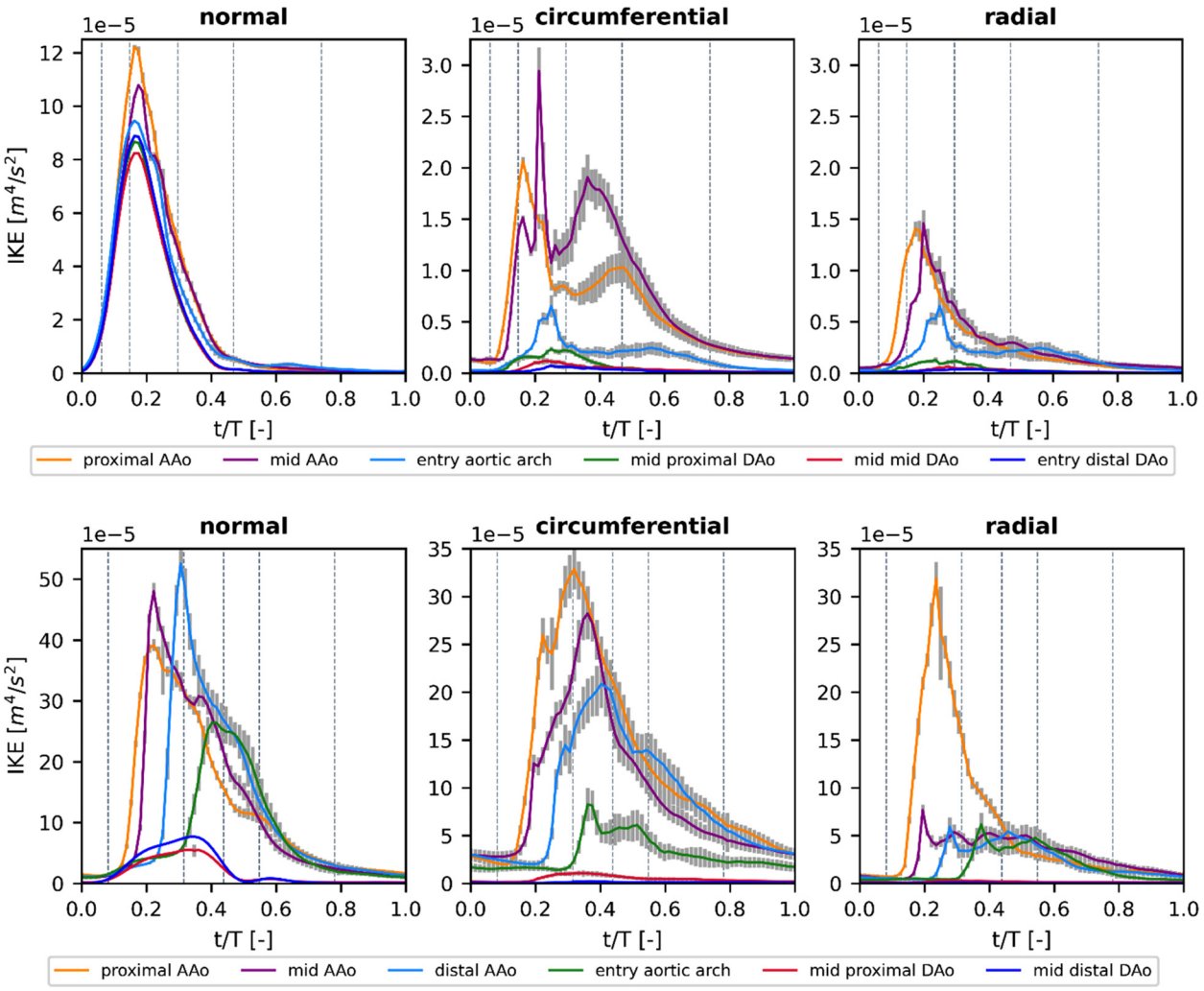


FIG. 4. Distribution of the integrated kinetic energy (IKE) over the three spatial directions, normal, circumferential, and radial, for the healthy aorta (top row) and aorta with AVS (bottom row). The colored lines indicate the phase-averaged values, while the gray bars indicate the standard deviation among the cardiac cycles. For orientation, the dashed vertical lines, in the respective order, indicate the time points of mid-systolic acceleration, peak systole, mid-systolic deceleration, end-systole, and mid-diastole.

direction. Elevated cycle variations remain present in the aortic arch and decrease significantly only in the DAo, where the energy of in-plane motion is an order of magnitude lower than in the AAo.

C. Kinetic energy spectrum

1. Local kinetic energy spectra

The kinetic energy spectrum of flow in the normal direction was calculated at the center point of each cross section. Figure 5 shows these spectra for the healthy aorta and for the aorta with AVS.

As aortic flow is of pulsatile or periodic nature, the frequency components of the kinetic energy can be divided into two groups. First, there are the frequencies which are multiples of the underlying cardiac cycles, also called the harmonics of the cardiac cycle. In Fig. 5 the harmonics are highlighted by the vertical dashed lines, where the first line, at $f_{h0} = 1.23$ and 1.37 Hz for the healthy and diseased aorta, respectively, is the so-called fundamental harmonic. An increase in the amplitudes of all harmonics above the fourth harmonic takes place from the proximal- to the mid-AAo, while at the same time, the lower harmonics show a decrease in their amplitudes. Going further down in the aorta, the amplitudes of the high harmonics decrease again and in the distal DAo, the kinetic energy is eventually concentrated in the first four to five harmonics. In the spectra of the aorta with AVS, a similar pattern is found in the distal DAo as the kinetic energy has again concentrated in the lower harmonics, up to the third harmonic. In contrast to the healthy aorta, along the center of the AAo, however, considerably lower amplitudes at lower harmonics are found.

While the flow composed of the harmonics is the same in all cardiac cycles, the second and much bigger group of the frequencies which lie in between the harmonics is the result of flow variations between different cardiac cycles. In other words, all energy from non-periodic, chaotic, and irregular motion, including turbulent motion, is

09 May 2024 15:22:56

© Author(s) 2024

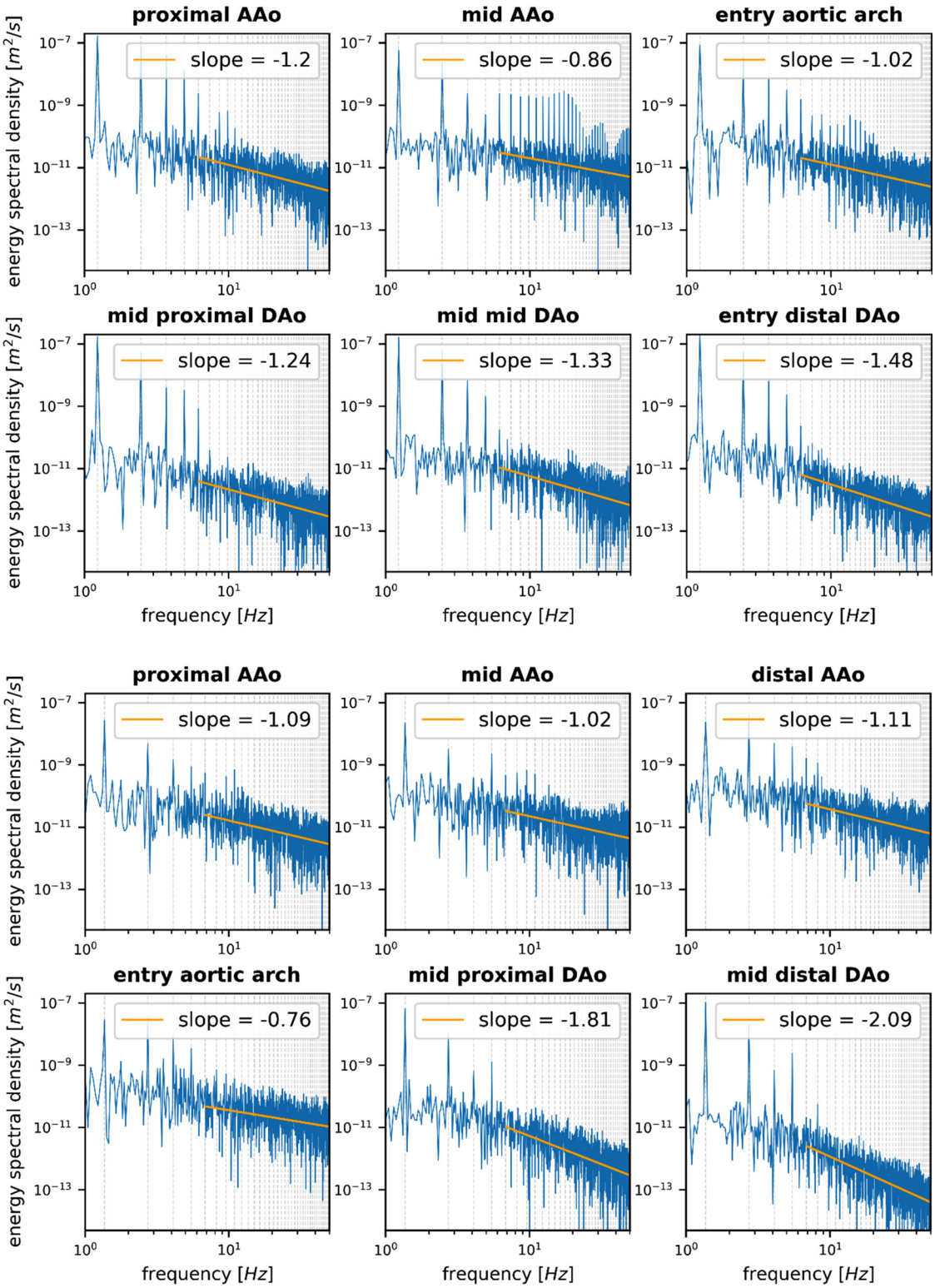


FIG. 5. Normal kinetic energy spectrum at the center points of the respective cross sections for the healthy aorta (top two rows), and the 7aorta with AVS (bottom two rows). The vertical dashed lines indicate the harmonics of the respective cardiac cycle.

09 May 2024 15:22:56

© Author(s) 2024

contained in this group of frequencies. To evaluate the dissipation and transfer of kinetic energy, also referred to as the kinetic energy cascade, the slope of the overall linearly decreasing amplitudes at higher frequencies is determined as shown in the spectra of Fig. 5. Generally, a higher slope means more kinetic energy is contained in higher frequency components and the turbulence reflected by the KES is more energetic. The frequencies lower than the fourth harmonic were excluded from the least squares fitting of the linear function because they were assumed to be responsible for the constitution of the periodic base flow as well as possible large-scale motions. Considering the slopes of the spectra in the healthy aorta, after an initial increase from the proximal- to the mid-AAo, a gradual decline is present toward the distal DAo. In contrast, in the aorta of the patient with AVS, the slope remains somewhat constant over the AAo, and after a small maximum at the entry to the aortic arch, it decreases gradually. Although this decrease is present in both aortas, it is more rapid, and much steeper gradients are reached in the aorta with AVS.

2. Spatial variation of the KES slopes

To avoid the interpretation based only on one single isolated spectrum at the center point, the KES and corresponding slopes were determined for all points within the cross sections. The resulting pseudo color maps of the slopes are shown in Fig. 6.

Comparing the cross sections located at similar positions in the proximal DAo of the healthy aorta and the aorta with AVS, higher slopes are present over a more extended region in the healthy aorta. This demonstrates that the higher slope in the DAo of the healthy aorta found in the isolated spectra of Fig. 5 is not an outlier. However, it can also be seen that the regions of higher slopes are smaller and of a lower level than the extended areas of high slopes found in the AAo of both cases.

3. Accumulated kinetic energy spectra

Indicated by the high spatial variation of slopes, the overall KES shapes can be assumed to be vastly different even within cross sections. However, a study of isolated local KES, as shown in Fig. 5, at different locations would quickly become cluttered. To gain an understanding of the distribution of KES shapes within a cross section, the individual local KES can be aggregated in intensity maps. For each frequency component, the intensity value reflects the ratio of the number of discrete points with a certain amplitude of energy spectral density to the total number of discrete points in a cross section. Here the overall amplitude range is divided into 1000 logarithmically spaced sections. In other words, the intensity maps indicate whether kinetic energy is accumulated in a narrow amplitude range or if the amplitudes are spread over a large energy spectral density range. The wider the spread, the more the shapes of the KES within the cross section are varying. Figure 7 shows the intensity maps of the KES of flow in the normal direction for all cross sections of the two aortas.

Similar to the local KES, the intensity map can be divided into two distinctive parts: the harmonics of the cardiac cycle and the intermediate frequencies. In the AAo, harmonics up to the highest frequencies are distinctive and the intensity is stretched over a wider range of energy spectral density levels, recognizable by the longer bright lines. Conversely, in the DAo, the peaks at higher harmonics have merged with the intermediate frequencies and the intensity in lower harmonics is concentrated in a narrower range of energy spectral density levels, resulting in the red almost dot-like short lines at the top of the peaks. This can be observed in the intensity maps of both aortas, and, additionally, a similar number of peaks at harmonics are distinctive. The intermediate frequencies, however, form a band that changes significantly from the cross sections in the AAo to the cross sections in the DAo, of both aortas. In the AAo, the band is rather narrow, e.g., clearly confined over the whole frequency range, while in the DAo, the band becomes wider and appears more blurred toward the higher frequencies. At the same time, it is apparent that the decline of the band toward higher frequencies is considerably slower in the AAo than in the DAo.

IV. DISCUSSION

A. Velocity field

In the healthy aorta, the vortex-like structure and its effect on the overall flow field in the AAo are consistent with the presence of

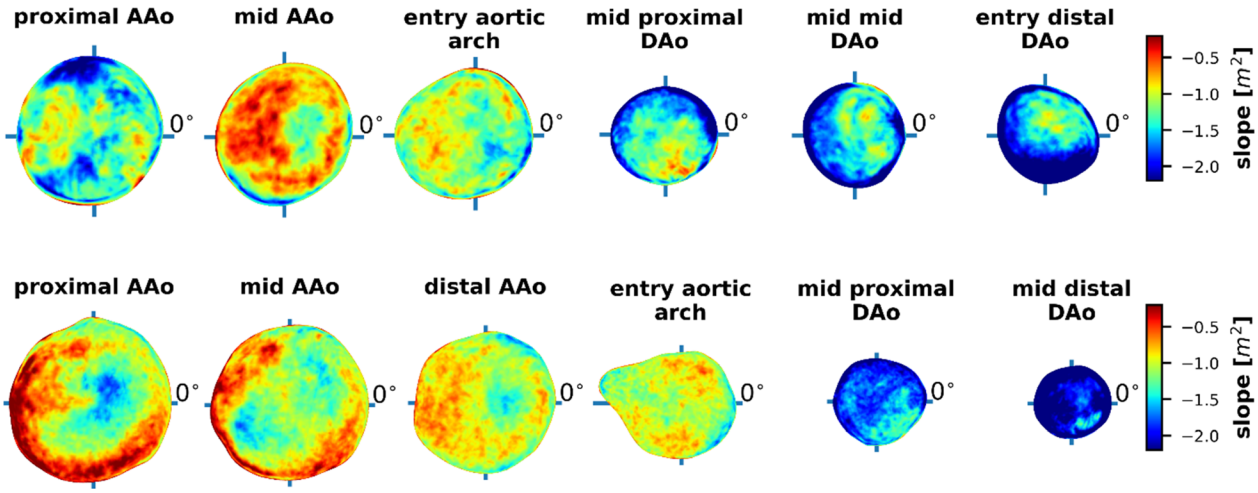


FIG. 6. Pseudo color maps showing the slope of the kinetic energy spectra, considering all frequency components starting from the fourth harmonic. The top row shows the cross sections from the healthy aorta, and the bottom row the respective cross sections from the aorta with AVS. The slope of the kinetic energy spectra varies significantly also within individual cross sections, indicating regions of stronger and weaker flow disturbances at higher frequencies.

09 May 2024 15:22:56

© Author(s) 2024

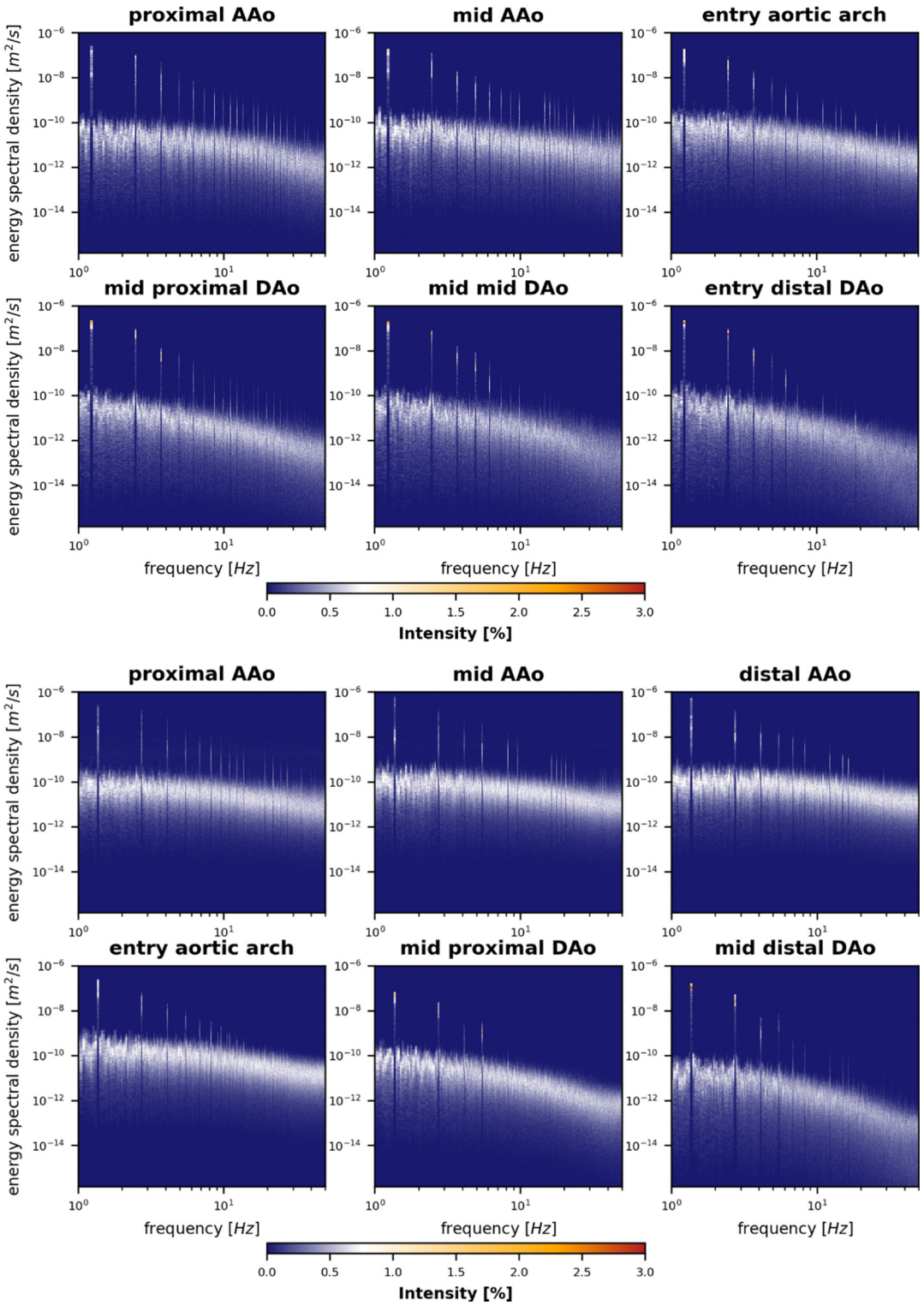


FIG. 7. Color maps of the intensity of kinetic energy levels of flow in normal direction at corresponding frequencies for the various cross sections of the healthy aorta (top two rows) and aorta with AVS (bottom two rows). The spectral distribution of kinetic energy can be divided into two groups of frequencies: the harmonics and the intermediate frequencies. While the harmonics constitute the periodic baseflow, the turbulent fluctuations are reflected in the intermediate frequencies.

09 May 2024 15:22:56

© Author(s) 2024

secondary and helical flows,[5,6,39] vortical structures,[8] and systolic backflow[5,7] reported in various studies. Furthermore, the existence of a recirculation zone[9] and double spiral flow,[11] also called Dean vortices, have been observed before. The strong and inclined jet out of the aortic valve due to the AVS[15,40] and the subsequent strong helical flow[14,15] are well-studied phenomena and commonly found with this pathology. Overall, the complex flow features and the resulting flow fields in both aortas are in very good agreement with the mentioned previous studies, confirming that the LES results provided realistic transient velocity fields of aortic blood flow.

B. Directional distribution

The IKE as a measure for the directional distribution of the instantaneous energy at different cross sections proves to be of valuable meaning, especially when interpreted with knowledge about the various flow features. The vortex structure in the AAo of the healthy patient is reflected through the delayed increase in IKE in the in-plane directions and its breakdown results in a sharp peak of the IKE in the mid-AAo. At this time point, above 20% of the total instantaneous IKE is in the in-plane motion. The broad peaks around end-systole and the following gradual decrease in IKE in the circumferential direction during diastole in the AAo are characterized by high cycle variations. This indicates that the vortex breakdown indeed causes a disturbed, irregular, and thus turbulent flow. Although the proportion of IKE in the in-plane directions is significantly smaller in the DAo, its normalization with the cross-sectional area, provided in the supplementary material, shows that considerable cycle variations remain. These can be interpreted as the result of disturbance caused by the interference between the remains of the vortex structure in the AAo and the recirculation and double-spiral flow in the DAo. In the aorta with AVS, the inclined inflow jet in the proximal AAo is reflected by the extreme magnitude of the peak IKE in the radial direction. At peak systole, 70% of the total IKE is present in the in-plane velocity components, highlighting the dominance of the inclined jet. The shift of the peaks of IKE in normal and circumferential directions toward later times in the cardiac cycle at subsequent cross sections in the AAo, is a direct result of the helical motion. However, through the decrease in IKE in circumferential and an increase in the normal direction toward the aortic arch, it is also apparent that the energy is gradually directed in the normal direction. The highest cycle variations in IKE in the AAo with AVS are present after peak systole and last well into diastole. This is in good agreement with the finding reported by Manchester *et al.*[16] that the turbulent kinetic energy remained elevated for longer time in the cardiac cycle than the mean kinetic energy.

C. Spectral distribution

The characteristic distinction of the harmonics and the intermediate frequencies, found in the KES, was observed previously by Holdsworth *et al.*[41] in a single spectrum from the common carotid artery. This is the first study to report and evaluate the changes observed in both groups of frequencies over the extent of the aorta. While the distinction is apparent in both the individual spectra and the intensity maps, it is the latter that provides the holistic picture of the role of the harmonics. In the intensity maps from the AAo of both patients, the harmonics up to the highest considered are noticeable and at lower harmonics, the intensity is spread over a wide range of amplitudes. This reflects the complexities of the flow field in the AAo, such as the vortex structure in the AAo of the healthy patient, which is constituted by many harmonics and amplitudes. In the aorta of the patient with AVS, the dominance of the helical motion is additionally identified through higher amplitudes at low harmonics in the intensity maps of the circumferential motion, provided in the supplementary material. In the DAo of both cases, the fundamental and first three to four harmonics remain particularly distinctive in the sense that their amplitudes are limited to a narrow range, resulting in the red more dot-like peaks. This can be understood as a direct characteristic of the more uniform plug-like and less complex flow found in both DAo.

Concerning the band of intermediate frequencies and the characteristic gradual decline of amplitudes toward higher frequencies, it is important to remind that even the KES of a perfect laminar flow would show this pattern, but with the steepest slope possible. Generally, the frequency range captured in this study is associated with the production and transfer of kinetic energy. The change in the slope, therefore, reveals information about turbulence levels. Although in the AAo of both patients a wide range of slope values exists, coherent areas are observed that align well with the observed flow field. In the AAo of the healthy patient, the highest slopes are located in regions not occupied by the vortex structure. This can be explained through the strong irregular disturbances in the flow field and high cycle variance of the IKE, e.g., turbulent kinetic energy, which is primarily produced and dragged outward during the breakdown of the vortex. The overall decrease in the slopes in subsequent cross sections is in agreement with Saqr *et al.*[23] who, despite considering Womersley flow instead of 4D flow MRI-derived inlet profiles as in the present study, found that the slope decreases when moving downstream in a vessel, in their case from the aortic root to the thoracic aorta. The delayed onset of the continuous decrease in the slopes in the aorta of the patient with AVS is a direct cause of the strong helical motion that affects and disturbs the flow field beyond the aortic arch. However, with gradual redirection of the helical flow in the normal direction, areas of high slopes start to be more uniformly distributed, particularly visible at the entry to the aortic arch. In the proximal DAo, coherent regions of somewhat increased slopes are found in both aortas. Interestingly, however, the slopes are higher in the proximal DAo of the healthy patient. This suggests that the interference between the remains of the vortex structure in the AAo and the recirculation zone and the formation of the double-spiral flow in the DAo produces additional turbulent kinetic energy. In the aorta with AVS, no strong interference takes place as the formation of the double-spiral flow, particularly, is observed at a smaller magnitude. This is in good agreement with Zhang *et al.*[10] who found Dean vortices to be more pronounced in Romanesque aortic arches, to which the geometry of the healthy aorta is much closer.

According to Kolmogorov–Obukhov statistical theory of turbulence, which describes isotropic homogeneous turbulence based on fully developed turbulent flow, kinetic energy cascade follows scaling laws that define the rate of transfer of kinetic energy. Kolmogorov-type energy cascades, e.g., a slope close to $-5/3$ in the inertial subrange, have been reported in studies concerned with turbulence in the immediate wake of aortic valve replacements.[28,29] In the frequency range captured in this study, however, no adherence to the Kolmogorov's $-5/3$ power law can be found, as the slopes vary below or above this value. Similar observations have been reported by Saqr *et al.*[23] who evaluated the same frequency range and found non-Kolmogorov-type

09 May 2024 15:22:56

© Author(s) 2024

energy cascades in Womersley flow through various blood vessels. The findings of this study, therefore, independently support the hypothesis of Nitti *et al.*,[27] Saqr *et al.*,[23] and Lancellotti *et al.*[23] that turbulence in the aorta cannot be expected to be isotropic and that Kolmogorov's theory, therefore, is not applicable. This hypothesis is further substantiated by Cerbus *et al.*[42] who demonstrate that even in transitional flow in straight pipes, good proximity to the Kolmogorov $-5/3$ spectra is only found at Reynolds numbers above 80 000. Nevertheless, as in this LES-based study, which does not resolve the highest frequencies, only the lower frequency range is captured, hence no conclusive statement can be made as to whether non-Kolmogorov-type cascades are present through the whole inertial subrange.

D. Model limitations

The patient-specific LES results adopted in this study covered up to 30 cardiac cycles to ensure statistical convergence of turbulence parameters. To ensure computational affordability, it was necessary to accept simplifications of the aortic system, namely neglecting the non-Newtonian character of blood and the aortic wall compliance. However, it has been shown that the effect of a constant Newtonian viscosity is minor in medium and high-velocity ranges[43] and that the primary effect of the non-Newtonian character of blood is slight turbulence damping, rather than alteration of overall flow characteristics.[44] Additionally, it has been demonstrated that important flow patterns are well reproduced with rigid-wall models.[45] Furthermore, velocity fields obtained from the LES were validated against 4D flow MRI measurements, showing excellent agreement, and further details can be found in our previous publication[16] and in the supplementary material. In addition, blood flow was treated as a continuum and only lower frequencies, e.g., larger scales of motion, were considered in this study and any interference of smaller scales with blood cells[46] has, therefore, been ignored.

Due to the complexity of the discretized geometry and associated high data storage, the time step at which the transient velocity field could be saved in the LES output files was limited to 10 ms. This time step, however, defines the sampling frequency $f_s = 100$ Hz and, thus, the highest frequency component that can be decomposed to $f_s = 50$ Hz, also called the Nyquist frequency. Moreover, since MRI scanners are limited in their temporal resolution and the scans acquired in this study were sampled at 20 Hz, time steps in between recordings had to be linearly interpolated to obtain the time-resolved inlet profiles. Therefore, high-frequency fluctuations in the flow, observed in the aorta downstream of bioprosthetic valves between 40 and 70 Hz,[29,47] may also exist in normal physiological flow but cannot be captured by the inlet conditions adopted here.

V. CONCLUSION

By analyzing the directional and spectral distribution of kinetic energy in two different patient-specific aorta models, this study has provided fundamental insights into the characteristics of realistic aortic blood flow and associated turbulence. It has been found that, from the AAo to the DAo, the number of constituting harmonics decreases, and the slopes of the KES gradually decline, supporting the common understanding of the flow to be more complex in the AAo. However, the results also demonstrate the presence of disturbances and turbulent flow even in the DAo of a healthy aorta. The directional distribution of kinetic energy further demonstrates the significant proportion of secondary flow in the in-plane directions. Complex three-dimensional flow structures are found to be the main source of disturbances and turbulence, reflected not only in the variance of directional distributions of kinetic energy but also in the more than one order of magnitude higher kinetic energy at higher frequencies in the respective regions. In support of recent studies, the turbulence present in the aortas is found to be of non-Kolmogorov type.

The characteristic directional and spectral distributions of kinetic energy highlight similarities and differences in the flow field of the two examined aortas. The dominating helical motion and associated turbulence in the AAo of the aorta with AVS is reflected through a wider spread of energy spectral density at lower harmonics and a more confined and less steep band of intermediated frequencies, when compared to the KES of the healthy aorta. In the proximal- and mid-DAo, the reverse observation is made, as the inference of the double-spiral flow and recirculation zone, which are more developed in the healthy aorta, creates additional turbulence. However, the continuing accumulation of energy in a small range of energy spectral density in the lower harmonics indicates the approach of more plug-flow-like conditions in the DAo of both aortas. The fact that the characteristics and differences in the directional and spectral distribution of the kinetic energy between a healthy aorta and an aorta with AVS can be identified, raises the importance for future studies to clarify universality. It should further motivate future studies to determine the KES up to higher frequencies and obtain an even more holistic understanding of the spectral distribution of kinetic energy in the aorta and other blood vessels. Overall, this study demonstrates the relevance of incorporating these fundamental fluid dynamic analyses in studies of flow in blood vessels. It further supports the call of recent studies for a shift in perception toward the non-laminar, turbulent nature of healthy and diseased aortic blood flow.

SUPPLEMENTARY MATERIAL

See the supplementary material for further details on the applied Windkessel model outlet boundary conditions and the sensitivity analysis of the LES simulations. Additionally, the flow fields from the remaining cross sections, plots of the surface area normalized IKE, and the energy spectral density intensity maps for flow in the circumferential and radial direction are provided.

ACKNOWLEDGMENTS

E.M. was supported by a Ph.D. scholarship through the EPSRC Doctoral Training Partnership grant to Imperial College London (EP/R512540/1). This work used the Cirrus UK National Tier-2 HPC Service at EPCC (http://www.cirrus.ac.uk) funded by the University of Edinburgh and EPSRC (EP/P020267/1). MR images used in the original computational simulations were provided by Declan O'Regan, Hammersmith Hospital, MRC London Institute of Medical Sciences, Imperial College London.

AUTHOR DECLARATIONS

Conflict of Interest

The authors have no conflicts to disclose.

Author Contributions

David Büchner: Conceptualization (lead); Formal analysis (lead); Methodology (lead); Writing—original draft (equal); Writing—review

09 May 2024 15:22:56

© Author(s) 2024

& editing (equal). **Emily Louise Manchester:** Data curation (lead); Formal analysis (supporting); Methodology (supporting); Writing—review & editing (equal). **Xiao Yun Xu:** Conceptualization (supporting); Resources (lead); Supervision (lead); Writing—review & editing (equal).

DATA AVAILABILITY

The data that support the findings of this study are available from the corresponding author upon reasonable request.

REFERENCES

[1]S. Coffey, B. J. Cairns, and B. Iung, "The modern epidemiology of heart valve disease," Heart **102**(1), 75 (2016).
[2]K. Takahashi, T. Sekine, T. Ando, Y. Ishii, and S. Kumita, "Utility of 4D flow MRI in thoracic aortic diseases: A literature review of clinical applications and current evidence," Magn. Reson. Med. Sci. **21**(2), 327 (2022).
[3]S. Numata, K. Itatani, K. Kanda, K. Doi, S. Yamazaki, K. Morimoto, K. Manabe, K. Ikemoto, and H. Yaku, "Blood flow analysis of the aortic arch using computational fluid dynamics," Eur. J. Cardiothorac. Surg. **49**(6), 1578 (2016).
[4]M. D. Hope, T. A. Hope, S. E. S. Crook, K. G. Ordovas, T. H. Urbania, M. T. Alley, and C. B. Higgins, "4D flow CMR in assessment of valve-related ascending aortic disease," JACC: Cardiovasc. Imaging **4**, 781 (2011).
[5]K. L. Hansen, H. Møller-Sørensen, J. Kjaergaard, M. B. Jensen, J. T. Lund, M. M. Pedersen, T. Lange, J. A. Jensen, and M. B. Nielsen, "Analysis of systolic backflow and secondary helical blood flow in the ascending aorta using vector flow imaging," Ultrasound Med. Biol. **42**(4), 899 (2016).
[6]C. H. Lee, K. S. Liu, G. H. Jhong, S. J. Liu, M. Y. Hsu, C. J. Wang, and K. C. Hung, "Finite element analysis of helical flows in human aortic arch: A novel index," Biomicrofluidics **8**(2), 024111 (2014).
[7]M. Z. Bensalah, E. Bollache, N. Kachenoura, A. Giron, A. De Cesare, L. Macron, M. Lefort, A. Redheuill, and E. Mousseaux, "Geometry is a major determinant of flow reversal in proximal aorta," Am. J. Physiol. **306**, H1408 (2014).
[8]A. Frydrychowicz, A. Berger, A. Munoz del Rio, M. F. Russe, J. Bock, A. Harloff, and M. Markl, "Interdependencies of aortic arch secondary flow patterns, geometry, and age analysed by 4-dimensional phase contrast magnetic resonance imaging at 3 Tesla," Eur. Radiol. **22**, 1122 (2012).
[9]J. Lantz, R. Gårdhagen, and M. Karlsson, "Quantifying turbulent wall shear stress in a subject specific human aorta using large eddy simulation," Med. Eng. Phys. **34**(8), 1139 (2012).
[10]Y. Zhang, R. Zhang, N. Thomas, A. H. Ullah, B. Eichholz, J. Estevadeordal, and Y. B. Suzen, "Experimental and computational study of pulsatile flow characteristics in Romanesque and gothic aortic arch models," Med. Eng. Phys. **102**, 103784 (2022).
[11]P. A. Stonebridge, S. A. Suttie, R. Ross, and J. Dick, "Spiral Laminar Flow: a Survey of a Three-Dimensional Arterial Flow Pattern in a Group of Volunteers," Eur. J. Vasc. Endovasc. Surg. **52**(5), 674–680 (2016).
[12]R. Torii, M. Kalantzi, S. Theodoropoulos, P. Sarathchandra, X. Y. Xu, and M. H. Yacoub, "Predicting impending rupture of the ascending aorta with bicuspid aortic valve: Spatiotemporal flow and wall shear stress," JACC: Cardiovasc. Imaging **6**, 1017 (2013).
[13]S. Pirola, O. A. Jarral, D. P. O'Regan, G. Asimakopoulos, J. R. Anderson, J. R. Pepper, T. Athanasiou, and X. Y. Xu, "Computational study of aortic hemodynamics for patients with an abnormal aortic valve: The importance of secondary flow at the ascending aorta inlet," APL Bioeng. **2**(2), 026101 (2018).
[14]K. Hansen, K. Lindskov, H. Møller-Sørensen, J. Kjaergaard, M. B. Jensen, J. A. Jensen, and M. B. Nielsen, "Aortic valve stenosis increases helical flow and flow complexity: A study of intra-operative cardiac vector flow imaging," Ultrasound Med. Biol. **43**(8), 1607 (2017).
[15]H. Ha, G. B. Kim, J. Kweon, S. J. Lee, Y. H. Kim, N. Kim, and D. H. Yang, "The influence of the aortic valve angle on the hemodynamic features of the thoracic aorta," Sci. Rep. **6**(1), 32316 (2016).
[16]E. L. Manchester, S. Pirola, M. Y. Salmasi, D. P. O'Regan, T. Athanasiou, and X. Y. Xu, "Analysis of turbulence effects in a patient-specific aorta with aortic valve stenosis," Cardiovasc. Eng. Technol. **12**, 438 (2021).
[17]J. H. Yen, S. F. Chen, M. K. Chern, and P. C. Lu, "The effect of turbulent viscous shear stress on red blood cell hemolysis," J. Artif. Organs **17**, 178 (2014).
[18]P. F. Davies, A. Remuzzi, E. J. Gordon, C. Forbes Dewey, Jr., and M. A. Gimbrone, Jr., "Turbulent fluid shear stress induces vascular endothelial cell turnover in vitro," Proc. Natl. Acad. Sci. U. S. A. **83**, 2114 (1986).
[19]E. L. Manchester, S. Pirola, S. Pirola, G. Mastroiacovo, G. Polvani, G. Pontone, and X. Y. Xu, "Aortic valve neocuspidization and bioprosthetic valves: Evaluating turbulence haemodynamics," Comput. Biol. Med. **171**, 108123 (2024).
[20]K. Bäumler, V. Vedula, A. M. Sailer, J. Seo, P. Chiu, G. Mistelbauer, F. P. Chan, M. P. Fischbein, A. L. Marsden, and D. Fleischmann, "Fluid–structure interaction simulations of patient-specific aortic dissection," Biomech. Model. Mechanobiol. **19**, 1607 (2020).
[21]J. Lantz, T. Ebbers, J. Engvall, and M. Karlsson, "Numerical and experimental assessment of turbulent kinetic energy in an aortic coarctation," J. Biomech. **46**, 1851 (2013).
[22]C. W. Ong, I. Wee, N. Syn, S. Ng, H. L. Leo, A. M. Richards, and A. M. T. L. Choong, "Computational fluid dynamics modeling of hemodynamic parameters in the human diseased Aorta: A systematic review," Ann. Vasc. Surg. **63**, 336 (2020).
[23]K. M. Saqr, S. Tupin, S. Rashad, T. Endo, K. Niizuma, T. Tominaga, and M. Ohta, "Physiologic blood flow is turbulent," Sci. Rep. **10**(1), 15492 (2020).
[24]R. M. Lancellotti, C. Vergara, L. Valdettaro, S. Bose, and A. Quarteroni, "Large eddy simulations for blood dynamics in realistic stenotic carotids," Numer. Methods Biomed. Eng. **33**(11), e2868 (2017).
[25]V. Mancini, A. W. Bergersen, J. Vierendeels, P. Segers, and K. Valen-Sendstad, "High-frequency fluctuations in post-stenotic patient specific carotid stenosis fluid dynamics: A computational fluid dynamics strategy study," Cardiovasc. Eng. Technol. **10**, 277 (2019).
[26]A. Fuchs, N. Berg, and L. P. Wittberg, "Pulsatile aortic blood flow—A critical assessment of boundary conditions," J. Eng. Sci. Med. Diagn. Ther. **4**(1), 011002 (2021).
[27]A. Nitti, G. De Cillis, and M. D. de Tullio, "Numerical investigation of turbulent features past different mechanical aortic valves," J. Fluid Mech. **940**, A43 (2022).
[28]L. Pietrasanta, S. Zheng, D. De Marinis, D. Hasler, and D. Obrist, "Characterization of turbulent flow behind a transcatheter aortic valve in different implantation positions," Front. Cardiovasc. Med. **8**, 804565 (2022).
[29]B. Becsek, L. Pietrasanta, and D. Obrist, "Turbulent systolic flow downstream of a bioprosthetic aortic valve: Velocity spectra, wall shear stresses, and turbulent dissipation rates," Front. Physiol. **11**, 577188 (2020).
[30]S. Tupin, K. M. Saqr, S. Rashad, K. Niizuma, M. Ohta, and T. Tominaga, "Non-Kolmogorov turbulence and inverse energy cascade in intracranial aneurysm: Near-wall scales suggest mechanobiological relevance," arXiv:2001.08234 (2020).
[31]P. D. Stein and H. N. Sabbah, "Turbulent blood flow in the ascending aorta of humans with normal and diseased aortic valves," Circ. Res. **39**(1), 58 (1976).
[32]E. L. Manchester and X. Y. Xu, "The effect of turbulence on transitional flow in the FDA's benchmark nozzle model using large-eddy simulation," Numer. Methods Biomed. Eng. **36**(10), e3389 (2020).
[33]S. Pirola, Z. Cheng, O. A. Jarral, D. P. O'Regan, J. R. Pepper, T. Athanasiou, and X. Y. Xu, "On the choice of outlet boundary conditions for patient-specific analysis of aortic flow using computational fluid dynamics," J. Biomech. **60**, 15 (2017).
[34]E. L. Manchester, S. Pirola, M. Y. Salmasi, D. P. O'Regan, T. Athanasiou, and X. Y. Xu, "Evaluation of computational methodologies for accurate prediction of wall shear stress and turbulence parameters in a patient-specific aorta," Front. Bioeng. Biotechnol. **10**, 836611 (2022).
[35]K. Jarvis, J. T. Pruijssen, A. Y. Son, B. D. Allen, G. Soulat, A. Vali, A. J. Barker *et al.*, "Parametric hemodynamic 4D flow MRI maps for the characterization of chronic thoracic descending aortic dissection," Magn. Reson. Imaging **51**(5), 1357 (2020).
[36]M. D. Powell and T. A. Reinhold, "Tropical cyclone destructive potential by integrated kinetic energy," Bull. Am. Meteorol. Soc. **88**, 513 (2007).

09 May 2024 15:22:56

© Author(s) 2024

[37]B. F. Klose, G. B. Jacobs, and A. Kopriva, "Assessing standard and kinetic energy conserving discontinuous Galerkin formulations for marginally resolved Navier-Stokes flows," arXiv:1910.13985 (2019).
[38]L. A. El-Gabry, D. R. Thurman, and P. E. Poinsatte, "Procedure for determining turbulence length scales using hotwire anemometry," Report No. GRC-E-DAA-TN4063, 2014.
[39]D. Li, J. Wang, W. Zeng, X. Zeng, Z. Liu, H. Cao, D. Yuan, and T. Zheng, "The loss of helical flow in the thoracic aorta might be an identifying marker for the risk of acute type B aortic dissection," Comput. Methods Programs Biomed. **230**, 107331 (2023).
[40]A. P. Yoganathan, "Fluid mechanics of aortic stenosis," Eur. Heart J. **9**, 13 (1988).
[41]D. W. Holdsworth, C. J. D. Norley, R. Frayne, D. A. Steinman, and B. K. Rutt, "Characterization of common carotid artery blood-flow waveforms in normal human subjects," Physiol. Meas. **20**, 219 (1999).
[42]R. T. Cerbus, C. C. Liu, G. Gioia, and P. Chakraborty, "Small-scale universality in the spectral structure of transitional pipe flows," Sci. Adv. **6**, eaaw6256 (2020).
[43]A. D. Caballero and S. Laín, "Numerical simulation of non-Newtonian blood flow dynamics in human thoracic aorta," Comput. Methods Biomech. Biomed. Eng. **18**, 1200 (2015).
[44]M. Andersson, J. Lantz, |T. Ebbers, and M. Karlsson, "Quantitative assessment of turbulence and flow eccentricity in an aortic coarctation: Impact of virtual interventions," Cardiovasc. Eng. Technol. **6**(3), 281 (2015).
[45]S. Jin, J. Oshinski, and D. P. Giddens, "Effects of wall motion and compliance on flow patterns in the ascending aorta," J. Biomech. Eng. **125**(3), 347 (2003).
[46]L. Antiga and D. A. Steinman, "Rethinking turbulence in blood," Biorheology **46**(2), 77 (2009).
[47]E. L. Johnson, M. R. Rajanna, C. H. Yang, and M. C. Hsu, "Effects of membrane and flexural stiffnesses on aortic valve dynamics: Identifying the mechanics of leaflet flutter in thinner biological tissues," Forces Mech. **6**, 100053 (2022).

09 May 2024 15:22:56

© Author(s) 2024